Available online at www.sciencedirect.com

ScienceDirect

Advances in Space Research 72 (2023) 2759–2777

ADVANCES IN SPACE RESEARCH (a COSPAR publication)

www.elsevier.com/locate/asr

Covariance determination for improving uncertainty realism in orbit determination and propagation

Alejandro Cano [a,b,*], Alejandro Pastor [b], Diego Escobar [b], Joaquín Míguez [a], Manuel Sanjurjo-Rivo [a]

[a] Universidad Carlos III de Madrid, Avenida Universidad 30, Leganés 28911, Spain
[b] GMV, Calle Isaac Newton 11, Tres Cantos 28670, Spain

Received 31 December 2021; received in revised form 22 July 2022; accepted 1 August 2022
Available online 5 August 2022

Abstract

The reliability of the uncertainty characterization, also known as uncertainty realism, is of the uttermost importance for Space Situational Awareness (SSA) services. Among the many sources of uncertainty in the space environment, the most relevant one is the inherent uncertainty of the dynamic models, which is generally not considered in the batch least-squares Orbit Determination (OD) processes in operational scenarios. A classical approach to account for these sources of uncertainty is the theory of consider parameters. In this approach, a set of uncertain parameters are included in the underlying dynamical model, in such a way that the model uncertainty is represented by the variances of these parameters. However, realistic variances of these consider parameters are not known a priori. This work introduces a methodology to infer the variance of consider parameters based on the observed distribution of the Mahalanobis distance of the orbital differences between predicted and estimated orbits, which theoretically should follow a chi-square distribution under Gaussian assumptions. Empirical Distribution Function statistics such as the Cramer-von-Mises and the Kolmogorov–Smirnov distances are used to determine optimum consider parameter variances. The methodology is presented in this paper and validated in a series of simulated scenarios emulating the complexity of operational applications.

Keywords: Uncertainty realism; Covariance realism; Space situational awareness; Covariance determination; Mahalanobis distance; Chi-square distribution; Cramer-von-Mises; Kolmogorov–Smirnov

1. Introduction

The provision of most of the services in Space Traffic Management (STM) and SSA relies on the proper characterization of the orbital uncertainty. This is known as uncertainty realism, and focuses on the correct representation of the Probability Density Function (PDF) of the orbital state. Uncertainty realism can be reduced to covariance realism under Gaussian assumptions, requiring not only an unbiased estimation but also covariance consistency (correct covariance orientation, shape, and scale). When these requirements are met, the PDF representing the uncertainty of the system can be fully characterized by its two first moments, gathered in a state and its associated covariance matrix. These are strong assumptions, though widely applied in operational SSA environments, where Resident Space Objects (RSOs) uncertainty is represented by the state and its associated covariance. Thus, covariance

* Corresponding author at: Universidad Carlos III de Madrid, Avenida Universidad 30, Leganés 28911, Spain.
E-mail addresses: alejandro.cano@alumnos.uc3m.es, alcano@gmv.com (A. Cano), apastor@gmv.com (A. Pastor), descobar@gmv.com (D. Escobar), jmiguez@ing.uc3m.es (J. Míguez), msanjurj@ing.uc3m.es (M. Sanjurjo-Rivo).

https://doi.org/10.1016/j.asr.2022.08.001
0273-1177/

realism can be understood as a necessary but not sufficient condition for uncertainty realism. The misrepresentation of the uncertainty of a RSO impacts STM and SSA products, being crucial for various tasks: RSO cataloguing, collision risk assessment, fragmentation analysis, re-entry prediction, track association, manoeuvre detection or sensor tasking and scheduling, among others. Many existing Orbit Determination processes are based on weighted batch least-squares theory and provide the estimation (state and covariance) as the nominal output, given that measurements are sufficient and available. Along this process, the dynamical model defining the motion of the orbiting object is assumed to be deterministic, and the estimation accuracy is determined considering only the uncertainty of the observations (Tapley et al., 2004). The resulting covariance matrix in this estimation process is known as the noise-only covariance (Montenbruck and Gill, 2000). However, one of the main sources of uncertainty during OD and subsequent propagation arises from the errors in the underlying dynamical models, which are typically disregarded (Alfriend et al., 2000; Montenbruck and Gill, 2000). For instance, when the ballistic coefficient is estimated in an OD process, the uncertainty of the atmospheric model is not considered, and thus the induced uncertainty on the rest of the state is not accounted for during the orbit determination and propagation. This results in overly-optimistic noise-only covariance matrices, which causes the covariance realism to degrade since the atmospheric density uncertainty will have an impact on the uncertainty of the estimated state, especially in the along-track position direction (Vallado, 1997).

Therefore it is customary, for SSA and particularly for Space Surveillance and Tracking (SST) purposes, to characterize and determine the inherent uncertainty in the dynamic or measurement models and their effects, which is commonly known as uncertainty quantification (UQ). Two fundamental problems can be distinguished for uncertainty quantification. On the one hand, the quantification of the uncertainty present in the system models, parameters, or data, also known as the inverse problem or inverse UQ (Poore et al., 2016). On the other hand, the propagation of uncertainty (UP). The latter concentrates on how to characterize the evolution of the system uncertainty, accurately and efficiently. Most UP methods focus on the propagation of an initially given Probability Density Function (PDF) of a state, though there exist methods for the propagation of epistemic uncertainty that do not rely on PDF propagation (Vasile, 2019). However, this is not the focus of the present work, where linearized propagation techniques are used. The inverse problem, on the contrary, consists in assessing the differences between the observed behaviour of a system and the underlying models and parameters used to represent it. This is the target of the work at hand.

Regarding the uncertainty in the modelling, a possible (not exclusive) approach is to revisit the deterministic assumption in the equations of motion. Specifically, one may account for the model uncertainty by introducing stochastic dynamics or process noise, exploring different stochastic modelling such as Brownian motion, Ornstein–Uhlenbeck or Gauss–Markov processes (Poore et al., 2016). The inverse problem also tackles the parameter uncertainty, this is, the modelling of uncertain parameter present in the dynamics or measurements equations. If the uncertain parameter (whether static or time-dependent) can be observed or estimated, it is possible to include its impact in the evolution of the differential equations of motion. In the end, the goal of parameter uncertainty modelling is not only the a posteriori quantification of the errors, but also to represent the relationship between the uncertain parameter and the state variance.

There exists a wide variety of techniques that target directly the complete inverse problem. Process noise methods, which consist in including additional noise terms in the dynamics to account for un-modelled error sources, are generally accepted over stochastic acceleration methods since they can account for both dynamic model and parameter uncertainty, especially if they are physically-based (Poore et al., 2016). However, many process noise solutions, based on noise fitting to observed orbital uncertainty, lack the physical meaning of the different sources of the uncertainty since they are focused on global process uncertainty rather than each individual source. For instance, process noise estimation via calibration process is proposed in (Duncan and Long, 2006; Schubert et al., 2021). Even though these techniques are typically used for filtering applications rather than in batch processing, some works describe the computation of a process noise matrix that accounts for the drag uncertainty and include it in the batch least-squares estimation process (Schiemenz et al., 2019). Other approaches suggest the use of empirical covariance matrices to include all residuals of the estimation process in the covariance computation, regardless of whether the uncertainty has been modelled or not (Frisbee, 2011; Cerven, 2011; Cerven, 2014). This proposal claims to account more accurately for noise time-variations rather than process noise or consider parameter analysis, at the expense of missing the physical interpretation of the uncertainty. Finally, particle filters are also a state-of-the-art technique that allows to retain higher moments of the target PDF by the selection of specific sigma points in pseudo Monte Carlo analysis (McCabe and DeMars, 2014). The key of these methods is the trade-off between accuracy and computational cost.

Therefore, uncertainty (and covariance) realism improvement is a direct consequence of reaching the UQ goals, this is, the characterization of the system uncertainty. However, apart from the aforementioned UQ methods, there are other techniques conceived to improve covariance realism without focusing on the sources of uncertainty and their modelling. For instance, state distribution in mean elements may be better represented by a multivariate normal distribution (Junkins et al., 1996; Vallado and Alfano, 2011). Other typical representations

of the state and covariance in non-linear reference frames that are able to slow down the realism degradation upon propagation are being widely studied, such as in Laurens et al. (2018). In an operational environment, operators require simple techniques in order to improve covariance realism since, as previously discussed, the nominal batch least-squares OD processes provide optimistic covariance estimations when only accounting for the measurements uncertainty. The most common options are: (1) the previously mentioned process noise and (2) scaling techniques, which inflate the covariance by means of scaling factors. Some authors propose the computation of such scaling based on increasing the initial position uncertainty to match the velocity error (Folcik et al., 2011). Others explore the use of the Mahalanobis distance of the orbital differences to find the scale factor (Laurens et al., 2017). However, a common drawback of artificially increasing the covariance is that the physical meaning of the correction is lost, not being able to understand the contributions of each source of uncertainty. These sort of methods based on artificially scaling the covariance matrix are used nowadays in operation centres such as the Space Operations Center (CSpOC) (Poore et al., 2016).

It is seen that simple and reliable UQ method that provide realistic characterization of the uncertainty are required by operators nowadays. One of the classical approaches for parameter UQ in the dynamic equations is the consider parameters theory, which can be classified within the process noise techniques (Montenbruck and Gill, 2000). It consists in extending the state space by including parameters in the dynamic models, such as atmospheric force, solar radiation pressure force or measurement models. These parameters are devised to follow a certain model with its corresponding uncertainty, e.g. a Gaussian distribution with a null mean (to maintain an unbiased estimation) and a certain variance. This allows the representation of unaccounted error sources of the dynamical or measurement models by including the parameter uncertainty. This formulation can be combined with batch estimation or filtering algorithms such as in the Schmidt-Kalman filter (Zanetti and D'Souza, 2013; Jazwinski, 1970). This approach provides the advantage of tracking the effect of the specific uncertain physically-based parameters that are included, as opposed to artificial scaling factors. However, one of the main drawbacks of the consider parameter theory is that realistic variances of such parameters are not normally known, a common problem in process noise methods. Overly optimistic, or oversized, variances may fail to model the uncertainty of parameters in the estimation and subsequent propagation of the covariance, not achieving covariance realism.

The aim of this work is to present a novel methodology to determine the variance of the considered parameters to improve the realism of the state covariance matrices obtained from operational OD processes. The method is based on the orbital differences between estimated and predicted orbits. Under Gaussian assumptions, the differences between both orbits projected into the covariance space, i.e. Mahalanobis distance, should follow a χ^2 distribution to achieve covariance realism. Thus, the variance of the consider parameters can be determined by means of a statistical comparison process between the observed Mahalanobis distance distribution and the expected one, i.e. a χ^2 distribution. We refer to estimated orbits as those ones obtained after an Orbit Determination process, backed up with observations. Predicted orbits refer to the propagation of those estimates with the same dynamical model to the future. The work carried out focuses on Low Earth Orbits (LEO) regimes, tackling some of the most relevant uncertainty sources such as the atmospheric density in the drag force acceleration, the range bias in the radar measurements or the solar proxies prediction (Vallado et al., 2014).

A precursor analysis based on the consider parameter theory to improve the covariance realism is performed in (Lopez-Jimenez et al., 2021). There, it is proposed to correct the noise-only covariance with a least squares fitting to a so-called observed covariance, the latter being obtained as an empirical covariance based on orbital differences from a statistically representative population of different orbit determinations. This approach has a main drawback. To compute such empirical covariance, orbital differences corresponding to multiple orbital positions and observation scenarios (observations geometry, number of measurements, etc) are mixed. In the work presented here, this issue is mitigated by the normalisation obtained with the Mahalanobis distance, which is the cornerstone of the work in this paper. The estimated covariance in a batch least-squared process is affected as well by the orbit position of the estimation epoch and the observation scenario. Thus, orbital differences normalized by their associated covariance (i.e. Mahalanobis distance) could be treated as samples from the same distribution, concretely as a χ^2 distribution under Gaussian assumptions if the covariance is realistic, since as discussed later, the Mahalanobis distance of each sample shall be constant in time under certain assumptions. Preliminary studies that analysed the applicability of this methodology to LEO or GEO regimes can be found in (Cano et al., 2021b; Cano et al., 2021a), respectively.

The remainder of the paper is organised as follows: in Section 2 the consider parameter theory is reviewed and the methodology is presented. In Section 3, the simulation process and environment are described. Next, the results of the proposed covariance determination methodology are shown in Section 4. The focus is placed on the physical interpretation of the consider parameter variances obtained and the level of covariance realism enhancement achieved. Finally, Section 5 summarizes the conclusions of this work and the future work to be performed.

2. Methodology

This section revisits in first place the consider parameters theory and its direct effect on the covariance computa-

tion. Then, the specific formulation derived to include the consider parameter theory in the Mahalanobis distance computation is described. Finally, the consider parameter models devised in this work are defined.

2.1. Consider parameters theory in batch least-squares algorithm for orbit determination

The complete description of the consider parameter theory (or consider covariance analysis, as termed by some authors) can be found in many references such as (Montenbruck and Gill, 2000; Tapley et al., 2004). For brevity, only the final derivation in the nominal batch least-squares process is described next. Let us define the estimated state vector as

$$\mathbf{y}_{\mathbf{est}} = \begin{pmatrix} \mathbf{r}(t) \\ \mathbf{v}(t) \\ \mathbf{p}(t) \end{pmatrix} \in \mathbb{R}^{n}_{y} \tag{1}$$

being $\mathbf{r}(t), \mathbf{v}(t)$ and n_y the position, velocity and estimated state dimension, respectively. $\mathbf{p}(t)$ represents the estimated parameters, either applied to the force or the measurement models. Typical examples of these parameters are the Drag Coefficient (C_d) in LEO orbits or the Solar Radiation Pressure Coefficient (C_r) in GEO. The consider parameters to be modelled in our system can be gathered in a consider parameter vector

$$\mathbf{y}_c = \begin{pmatrix} c_1 \\ \vdots \\ c_n \end{pmatrix} \in \mathbb{R}^{n}_{c} \tag{2}$$

where n_c is the number of consider parameters. They are defined to follow a Normal distribution of the form

$$c_i \sim \mathrm{N}\left(0, \sigma_i^2\right), i = 1, \cdots, n \tag{3}$$

The null mean definition allows the expected value of the orbit estimation to remain unbiased (Montenbruck and Gill, 2000). On the contrary, the covariance of the estimation is affected. Recalling the nominal batch least-squares estimation, the noise-only covariance is

$$\mathbf{P}_n = \left(\mathbf{H}_y^T \mathbf{W} \mathbf{H}_y\right)^{-1} \in \mathbb{R}^{n_y \times n_y} \tag{4}$$

where $\mathbf{H_y}$ corresponds to the Jacobian of the observations with respect to the estimated state, and $\mathbf{W}$ is the weighting matrix containing the confidence of each measurement and the possible correlation among the measurements. Then, the consider covariance results in:

$$\mathbf{P}_c = \mathbf{P}_n + \left(\mathbf{P}_n \mathbf{H}_y^T \mathbf{W}\right)\left(\mathbf{H}_c \mathbf{C} \mathbf{H}_c^T\right)\left(\mathbf{P}_n \mathbf{H}_y^T \mathbf{W}\right)^T \tag{5}$$

where $\mathbf{H}_c$ is the Jacobian of the observations with respect to the consider parameters and

$$\mathbf{C} = \begin{pmatrix} \sigma_1^2 & \cdots & 0 \\ \vdots & \ddots & \vdots \\ 0 & \cdots & \sigma_n^2 \end{pmatrix} \tag{6}$$

contains the variances of the consider parameters, where no correlation between them is assumed. Eq. (5) can be simplified to obtain

$$\mathbf{P}_c = \mathbf{P}_n + \mathbf{K}\mathbf{C}\mathbf{K}^T \in \mathbb{R}^{n_y \times n_y} \tag{7}$$

$$\mathbf{K} = \mathbf{P}_n\left(\mathbf{H}_y^T \mathbf{W} \mathbf{H}_c\right) \in \mathbb{R}^{n_y \times n_c} \tag{8}$$

where n_c is the number of consider parameters. Therefore, the consider covariance is obtained as the noise-only covariance plus a covariance correction, which depends linearly on the consider parameter variances.

2.2. Consider parameters effect in orbit propagation

The consider covariance is obtained at estimation epoch and models the effect of the uncertainty of the consider parameters that affect the estimation, regardless whether their uncertainty affects the force or the measurements model. However, our interest in enhancing the covariance realism extends also to the covariance propagation for SST purposes. In this paper, we assume linear propagation of the covariance matrix, as it is generally applied in most operational scenarios in SST. More complex and accurate uncertainty propagation methods are out of the scope of this work since Gaussianity is a cornerstone assumption in the proposed methodology. In this respect, Michael's normality tests can be applied to assess data linearity (Michael, 1983; Royston, 1993). A complete derivation of linear propagation theory can be found in many well-known references, such as (Montenbruck and Gill, 2000). First, let us define the extended state vector as

$$\mathbf{y}_{\mathbf{ext}} = \begin{pmatrix} \mathbf{r}(t) \\ \mathbf{v}(t) \\ \mathbf{p}(t) \\ c_1 \\ \vdots \\ c_n \end{pmatrix} \in \mathbb{R}^{n_y + n_c} \tag{9}$$

which is composed of the estimated parameters plus the consider parameters of our analysis. In the end, to account for the effect of the main dynamic parameters in the propagation of the state, it is required to integrate the variational equations. Its solution is the Extended State Transition Matrix (ESTM)

$$\begin{aligned}
&\mathbf{\Psi}(t,t_0) = \begin{pmatrix} \mathbf{\Phi}(t,t_0) & \mathbf{S}(t,t_0) \\ \mathbf{0} & \mathbf{I} \end{pmatrix} \\
&\mathbf{\Psi} \in \mathbb{R}^{(n_y+n_c)\times(n_y+n_c)} \\
&\mathbf{\Phi} \in \mathbb{R}^{6\times 6} \\
&\mathbf{S} \in \mathbb{R}^{6\times n_p} \\
&\mathbf{I} \in \mathbb{R}^{n_p\times n_p}
\end{aligned} \tag{10}$$

where:

- n_p is the number of dynamical parameters to consider during propagation, which in this case corresponds to the estimated dynamical parameters plus the consider parameters, excluding position and velocity, hence, $n_p = (n_y - 6) + n_c$
- $\mathbf{\Phi}(t,t_0)$ corresponds to the state transition matrix, which relates the position and velocity at any time t with respect to the initial state at time t_0.
- $\mathbf{S}(t,t_0)$ is the so-called sensitivity matrix, which contains the partial derivatives of the state vector with respect to the model dynamical parameters, both estimated and considered. These parameters are defined as constant in the dynamic model as is customary in many propagation methods (Tapley et al., 2004), though in this case having a certain variance that the proposed methodology intends to estimate.

The ESTM can be computed by solving numerically its associated partial differential equations as shown in Montenbruck and Gill (2000). The typical linear covariance propagation applying the state transition matrix would be

$$\mathbf{P}_n(t) = \mathbf{\Phi}(t,t_0)\mathbf{P}_n(t_0)\mathbf{\Phi}(t,t_0)^T \tag{11}$$

However, to account for the effect of the uncertainty of the consider parameters in our covariance propagation, we define the extended consider covariance

$$\mathbf{P}_{\mathbf{c_{ext}}}(t_0) = \begin{pmatrix} \mathbf{P}_c & \mathbf{0} \\ \mathbf{0} & \mathbf{C} \end{pmatrix} = \begin{pmatrix} \mathbf{P}_n + \mathbf{KCK}^T & \mathbf{0} \\ \mathbf{0} & \mathbf{C} \end{pmatrix} \in \mathbb{R}^{(n_y+n_c)\times(n_y+n_c)} \tag{12}$$

where in addition to the classical consider covariance, the uncertainty of the consider parameters is also explicitly included. Thus, the extended covariance at any time, using the ESTM, is

$$\mathbf{P}_{c_{ext}}(t) = \mathbf{\Psi}(t,t_0)\mathbf{P}_{c_{ext}}(t_0)\mathbf{\Psi}(t,t_0)^T \tag{13}$$

By using the ESTM, the effect of the uncertainty of the model parameters is mapped into the position and velocity covariance not only at estimation, but also along the propagation. Of course, depending on the choice of consider parameters, they may affect only the estimation process, the propagation process, or both. This is a relevant factor to take into account in the analysis, and is further discussed for each consider parameter. The goal of the work at hand is to determine the values of $\mathbf{C}$ so that the consider covariance realism is improved.

2.3. Specific consider parameters

In this section, the main consider parameters that have been modelled in our work are presented. All of them follow the definition of Eq. (3). The general methodology presented in Sections 2.1 and 2.2 allows to include any desired consider parameter in the dynamic or measurement model. A relevant benefit of this methodology is that each parameter can be defined to model a specific uncertainty source, tailored to any orbital regime, which in principle allows to maintain the trace of the error sources. However, this traceability can be compromised by the correlation between the different consider parameter models, which may lead to the contribution of each uncertainty source to be hard to decouple. Therefore, another target of the work presented here is to assess the ability of the proposed methodology to maintain such traceability.

2.3.1. Aerodynamic model consider parameter

The classical drag force equation including the aerodynamic model consider parameter is defined as:

$$\mathbf{a}_{\text{drag}} = -\frac{1}{2}\rho\frac{C_d A}{m}|\mathbf{v}_{\text{rel}}|^2\frac{\mathbf{v}_{\text{rel}}}{|\mathbf{v}_{\text{rel}}|}(1+c_{AE}) \tag{14}$$

where ρ is the atmospheric density, C_d the drag coefficient, A the cross-sectional area, m the object mass and $\mathbf{v}_{rel}$ is the relative speed vector of the object with respect to the atmosphere. Finally c_{AE} is the consider parameter, whose objective is to model the error in the atmospheric density and ballistic coefficient, containing C_d as well as mass and cross-sectional area uncertainty. The uncertainty of this parameter affects both the estimation and propagation arc.

2.3.2. Range bias

This parameter is included to represent possible errors in the measurements model and calibration process. In this case, the measurement model becomes

$$z^* = z + c_z \tag{15}$$

where z represents the range measurement and c_z is the range bias error consider parameter. Note that Eq. (15) could represent any other measurement retrieved from a sensor, which in the case of a typical radar for SST purposes includes azimuth and elevation angles, range and range rate. The purpose of this consider parameter is to model the variance of the range bias of the sensor network, modeled as constant for each OD arc. Even though a sensor network mean bias can be applied after sensor calibration using previous data, an error is committed in subsequent OD arcs. The uncertainty of such error is what the proposed range bias consider parameter aims to model.

2.3.3. Atmospheric proxies prediction consider parameter

The aim of this parameter is to represent another relevant source of uncertainty in LEO, related to the uncertainty associated to the prediction of the atmospheric $F_{10.7}$ or A_p proxies that are used to compute the

atmospheric density at future times. Not only the proxies observations may vary depending on the source, but also the predicted values error represent a relevant uncertainty source (Vallado and Kelso, 2013). The consider parameter c_{PE} model is introduced in the drag force, namely,

$$\mathbf{a}_{\text{drag}} = -\frac{1}{2}\rho\frac{C_d A}{m}|\mathbf{v}_{\text{rel}}|^2\frac{\mathbf{v}_{\text{rel}}}{|\mathbf{v}_{\text{rel}}|}\left(1 + c_{PE}\cdot t_{\text{pred}}\right) \tag{16}$$

where t_{pred} is the prediction time (days), thus, c_{PE} has units of frequency [$days^{-1}$]. The source of uncertainty to be modelled here is considered to be only present during the orbit propagation and proportional to the prediction time, which is defined to start the day the first forecasted proxy is used in the atmospheric model. Although such a model will not have an impact during the orbit estimation, its associated covariance will affect the propagation of the state via the ESTM. This leads to a dominance of this model error after long propagation intervals, allowing to decouple its contribution from other modeled uncertainty sources.

Observed space weather data from NOAA is applied during OD, assumed as true, whereas predicted proxies are used during propagation as is detailed in 3.4. It can be noted that, as concluded in other studies such as in Vallado and Kelso (2013), the observed space weather data has its own uncertainty, arising from different observations and data processing of the different space weather sources. In the work presented here, this uncertainty during orbit estimation is modeled as Gaussian, and thus, it is contained inside the aerodynamic model consider parameter previously defined.

2.4. Covariance determination method

2.4.1. Mahalanobis distance with consider covariance

The Mahalanobis distance (d_M) is a well-known statistical metric that describes how far a state $y(t)$ is from a certain reference $y_{ref}(t)$, projected into the covariance space (Mahalanobis, 1936). The squared Mahalanobis distance is:

$$d_M^2 = \left(\mathbf{y} - \mathbf{y}_{ref}\right)^T\left(\mathbf{P} + \mathbf{P}_{ref}\right)^{-1}\left(\mathbf{y} - \mathbf{y}_{ref}\right) \tag{17}$$

where $\mathbf{P}$ and $\mathbf{P}_{ref}$ are the covariance matrices of the state and the reference, respectively. Both matrices are computed from Eq. 13, each one using their corresponding estimated covariances and ESTM matrices. Note that the orbit used as reference can also suffer from model errors, and thus the consider parameter correction impact on its noise-only covariance must also be considered as in Eq. 13. Eq. 17 assumes that no correlation exists between both variables $\mathbf{y}$ and $\mathbf{y}_{\mathbf{ref}}$, though this is not guaranteed, for instance, when the sensor network is common to both state estimations. The assumption of no correlation between the state and the reference is found in other studies such as Poore et al. (2016) or Hill et al. (2012). In the work presented here, we also assume no correlation between the state and the reference, mitigating any possible correlation by ensuring that the computed reference orbit, $\mathbf{y}_{\mathbf{ref}}$, does not share any observation with the orbit state under analysis, $\mathbf{y}$. Nonetheless, the validity of this assumption is assessed during the simulation results provided in this work. In addition to this, the covariance of the reference can be neglected when it is several orders of magnitude smaller. This occurs when the used reference orbit is assumed perfect (without uncertainty) (Folcik et al., 2011; Sabol et al., 2010) or when their sources are known to be highly accurate such as Precise Orbit Determination outputs.

For simplicity, the reference covariance is omitted in the following equations, although it is considered in the computations when applicable. In order to introduce the consider parameter effect, we recall the definition of the extended state vector of Eq. (9) and combine Eqs. 12,13 with Eq. (17), which yields

$$d_M^2(t) = \Delta\mathbf{y}(t)^T\left(\mathbf{\Psi}(t,t_0)\begin{pmatrix}\mathbf{P}_n + \mathbf{KCK}^T & \mathbf{0}\\ \mathbf{0} & \mathbf{C}\end{pmatrix}\mathbf{\Psi}(t,t_0)^T\right)^{-1}\Delta\mathbf{y}(t) \tag{18}$$

where $\Delta\mathbf{y}(t) = \mathbf{y}_{\mathbf{ext}}(t) - \mathbf{y}_{\mathbf{ref}}(t)$. Eq. (18) allows to compute the Mahalanobis distance at any epoch along the propagation arc as a function of the consider parameter variances contained in matrix $\mathbf{C}$, assuming that a batch least-squares parameter estimation process has been performed, followed by a propagation step.

2.4.2. Consider parameters variance determination

Under linear and Gaussian assumptions, this is, when the differences between the state and the reference are normally distributed and the covariance is representative of such distribution (i.e. realistic), the squared Mahalanobis distance should follow a χ^2 distribution, whose detailed characteristics may be found in D'Agostino and Stephens (1986). Eq. (18) allows us to evaluate the Mahalanobis distance at any propagation epoch by computing the orbital differences between a predicted orbit and a reference. Thus, if a population of estimated (and later propagated) orbits are available, together with reference orbits, it is possible to look for the consider parameter variances in matrix $\mathbf{C}$ so that the squared Mahalanobis distance population resembles the expected theoretical χ^2 distribution. Hence, computing the consider parameter variances is reduced to a statistical comparison process, where the free variables are the variances of the consider parameters. The covariance determination process can be divided in three main steps:

1. For a population of orbits, perform an OD process to obtain the noise-only covariance and the components of matrix $\mathbf{K}$. Then propagate the estimated states to obtain the predicted orbits and the ESTM.

2. For each predicted orbit, compute the orbital differences at any desired propagation epoch comparing against a reference orbit.
3. With all the data from the orbits population to construct Eq. (18), obtain the consider parameters variance that minimizes a certain metric of statistical comparison between the observed squared Mahalanobis distance distribution and the χ^2 distribution. The different metrics and minimization solver are described in Section 2.4.4.

Therefore, the objective is to retrieve the consider parameter distribution that has affected the population of orbits. This can be done provided that a sufficient amount of samples is available, where 'sufficient' means that a prescribed accuracy target can be attained as a trade-off between accuracy and amount of data available. This is further discussed in Section 4.3. The methodology looks for orbits affected by errors that are modelled to follow the consider parameter definitions of Section 2.3, this is, each orbit is affected by a constant error, drawn from the proposed consider parameter distribution whose variance we aim to estimate. The diversity of errors observed in the population allows to determine the variance of the proposed consider parameters applying the proposed covariance determination methodology. If the variance of the parameters is properly captured and the proposed models are representative of the system uncertainty, we can correct the estimated covariance and improve the covariance realism, as is seen in Section 4. In that regard, if the methodology is demonstrated to provide satisfactory and accurate results, being able to decouple the consider parameters impact and any other orbit correlation, we can maintain the trace of the error sources and their tailored correction in the covariance matrix.

One of the final objectives of this methodology is its operational applicability. To obtain a population of orbits of a single object in a SSA scenario, where the data is scarce, we have to resort to orbits estimated at different epochs, with different space weather proxies or even observation geometry. This is the reason why we propose the Mahalanobis distance metric to unify the orbits population under the same distribution (i.e. χ^2). On the one side, we are comparing against a reference orbit, and on the other side we are normalizing such differences with a covariance matrix generated from an OD process that will be coherently affected by the same diversity of estimation epochs and OD conditions. In fact, the Mahalanobis distance for each orbit is expected to remain approximately constant under Gaussian assumptions and sufficiently linear dynamics (Sabol et al., 2010).

2.4.3. Reference orbit for Mahalanobis distance

An orbit to be used as reference is required to compute the Mahalanobis distance. In many studies, the reference orbit used for the Mahalanobis distance computations is an assumed true, errorless orbit (Folcik et al., 2011; Sabol et al., 2010). In the context of this work, this orbit is defined as the "true reference" and its covariance can be neglected. In real operations, these kind of references may be available as Precise Orbit Determination products, with orbit precision of the order of 1 cm. However, these solutions require the collaboration of the satellites for such precise computations.

Thus, these solutions are not generally available in most operational situations in SST, where non-collaborative RSO are the main targets. For this purpose, this work proposes to use estimated orbits as reference orbits to compare against the propagated ones. In other words, if measurements are available for a certain period of time, we can use measurements in the propagation arc of another orbit to determine a reference orbit, whose absolute estimation error is several orders of magnitude lower that the propagated orbit under analysis. This has been defined as the Operational reference orbit (see Fig. 1). As was discussed in Section 2.4.1, this operational reference has a non-negligible covariance since it is estimated after an orbit determination process. Therefore, its covariance must be included when computing the Mahalanobis distance. The process to generate the Operational reference orbit in the presented simulations is detailed later in Section 3.1.

Both types of reference orbits (the "true" and the "operational") are tested in this work. Achieving similar performances of the methodology when using any of these refereces is of paramount importance for the operational applicability of the proposed covariance determination method, as it would not require external and precise ephemeris to use as reference.

2.4.4. Statistical comparison metrics and solver

The statistical comparison process consists in comparing the Cumulative Distribution Function (CDF) of the observed squared Mahalanobis distances with the χ^2 distribution CDF of as many degrees of freedom (DOF) as the ones included in the Mahalanobis distance computation. This can be reduced to the minimization of an Empirical Distribution Function statistic (EDF). These kind of tests are based on measuring the discrepancy between the

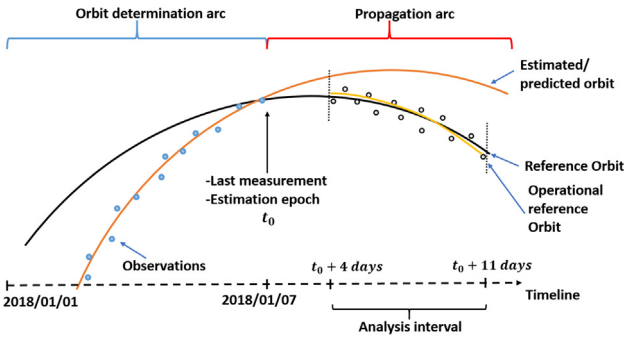

Fig. 1. Orbit estimation and propagation scheme for 1 Monte Carlo sample.

EDF (step function that approximates the CDF of a population) and a given function such as the χ^2. Among the multiple options available in the state-of-the-art (D'Agostino and Stephens, 1986; Poore et al., 2016), two relevant metrics are presented and compared along this work:

1. **Cramer-von-Mises (CvM)**: it is a quadratic statistic, based on the squared differences between both distributions, in this case with constant weights. A directly applicable formulation for the Cramer-von-Mises statistic to test if a given population $X_1, \cdots, X_n$ comes from a χ^2 distribution is

$$J = \frac{1}{12n} + \sum_{i=1}^{n} \left(\chi^2_{CDF}(X_i) - \frac{2i-1}{2n} \right)^2 \tag{19}$$

   where n is the total amount of samples, being sorted in increasing order. The null hypothesis of this test is that the candidate distribution belongs to the χ^2 distribution. Such hypothesis can be can be rejected with a 99.9% confidence level if the metric reaches values above 1.16 approximately. For a more robust applicability of such metric, upper tail correction factors as described in D'Agostino and Stephens (1986) can be applied.
2. **Kolmogorov–Smirnov (KS)**: it is a supremum statistic that consists in the maximum vertical difference between the empirical and theoretical CDFs, i.e.,

$$D = \max \left(\left| \chi^2_{CDF}(X_i) - \frac{i}{n} \right| \right) \tag{20}$$

   Again, n is the total amount of samples, sharing the same null hypothesis as the Cramer-von-Mises statistic. In this case, the null hypothesis can be rejected for metrics higher than 1.95 at same 99.9% confidence level. Again, tail correction factors can be applied.To minimize those metrics, the Differential Evolution algorithm (Storn et al., 1997) is applied, which consists in a heuristic approach for global multivariate function optimization, suitable also for nonlinear or non-differentiable functions. Instead of requiring an initial guess, this algorithm allows to define boundary regions for the optimized variables, in this case, the consider parameter variances. The boundaries applied for the consider parameter variances in all the simulations carried out in this work are shown in Table 1. As expected, the smaller the search region is, the faster the algorithm converges to the global solution. These values have been selected as a compromise between operational applicability and computational efficiency, representing a wide enough region to ensure that the unknown solution is contained, but maintaining physically logical upper boundaries.

Table 1
Minimisation boundaries

	σ_{AE} [%]	σ_{PE} [%/day]	σ_{RB} [m]
Upper bound	60	60	200
Lower Bound	0	0	0

3. Validation environment

3.1. Simulation scheme

To test the covariance realism improvement achieved with the proposed methodology, a validation campaign in a simulated environment has been carried out. The simulation process to generate a realistic environment is described next. Fig. 1 is included for further details of the process. It depicts a timeline of a Monte Carlo sample, consisting in an orbit determination and propagation process and differentiating between the reference orbit and the estimated/predicted orbit obtained during each process iteration.

- **True reference orbit:** it is obtained propagating a reference state associated to an existing RSO (see Table 2) from a certain reference epoch. The dynamic model of this propagation is deterministic and is not perturbed with randomly generated samples of the consider parameters (see Table 3 for further details). The length of this propagation arc is sufficient to cover all required arcs of posterior orbits.
- **Monte Carlo iterations**:
  - **Simulated orbit:** from the reference state, a propagation is performed over 7 days backwards from the estimation epoch (t_0), which are the nominal OD arcs of interest in LEO applications. Along this step, the aerodynamic model perturbation is included, obtaining a simulated orbit. Though for each sample the aerodynamic model perturbation (c_{AE}) is constant, each value is drawn from a Gaussian distribution with null mean and a simulated variance, following the consider parameter expectations of the perturbations. Recovering the input variance through our covariance determination methodology would serve as validation. The space weather information used

Table 2
Simulated reference RSO state.

Semi-major axis	7186.878 km
Eccentricity	0.001113
Inclination	98.72 °
RAAN	77.03 °
Arg of pericenter	111.436 °
True anomaly	71.98 °
Epoch (UTC)	2018–01-07 00:00:00.000
Mass	500 kg
SRP area	10 m^2
Drag area	10 m^2
Drag coefficient	2.0

Table 3
Dynamical model characteristics.

Reference frame	J2000 ECI
Gravity field	16x16
Third body perturbations	Sun & Moon
Earth geodetic surface	ERS-1
Polar motion and UT1	IERS C04 08
Earth pole model	IERS 2010 conventions
Earth precession/ nutation	IERS 2010 conventions
Atmospheric model	NLRMSISE-90
Solar radiation pressure	Constant area
Drag force	Constant area

along this step corresponds to observed proxies as provided by the Space Weather Prediction Center (NOAA), assumed to be the true proxies.

- **Tracks generation:** From such perturbed orbit, tracks are simulated from a ground-based sensor, in this case, corresponding to a LEO radar with similar visibility capabilities and accuracy as a real operational case (see Table 4 for the measurements noise and Table 5 for the radar characteristics). The range bias perturbation (c_{RB}) is introduced in this step analogously to the previous perturbation. An example of the resulting observations can be seen in Fig. 1. Approximately, between 8 to 10 tracks are generated, of around 2 min of duration each, providing between 750 and 1000 measurements (range, range-rate, azimuth an elevation). These numbers vary from one iteration to the next one due to the visibility intervals (orbit revisit period and orbit geometry).
- **Orbit determination and propagation:** an OD is performed with the simulated measurements, again with a 7 days determination arc. The estimated state is then propagated forward 11 days from the estimation epoch (t_0), corresponding to the last measurement, obtaining the predicted orbit and the extended state transition matrix. To realistically introduce the effect of the uncertainty in the solar proxies prediction (c_{PE}), true proxies are used only up to the estimation epoch, and as in daily satellite operations, algorithms for the prediction of space weather proxies are used complete the required set. Further details about this prediction are given in Section 3.4.
- **Operational reference orbit:** as previously defined, the purpose of this orbit is to check whether the methodology works when using a reference orbit that has been obtained in an orbit determination process. To this end, tracks are simulated as if the True reference orbit was observed, again with the same sensor network. Another OD process is performed using this new set of measurements and the true space weather proxies. For consistency, the length of the determination arc of this orbit is set to coincide with the determination arc of the orbit under analysis, equal to 7 days. The tracks generation and OD arc in this case is set to range from $t_0 + 4$ up to $t_0 + 11$, which corresponds to the interval of interest for our orbit comparisons and covariance matrix correction. Recall that t_0 is defined from the previously estimated/propagated orbit. Fig. 1 depicts this process. It is important to notice that this Operational reference orbit has a certain non-negligible covariance matrix as part of the OD process that needs to be included in the Mahalanobis distance computation.

Table 4
Measurement noise considered.

Measurement type	σ	Units
Two-way range (ground-satellite)	10	m
Two-way range rate (ground-satellite)	300	mm/s
Satellite azimuth and elevation	1	°

Table 5
Characteristics of simulated radar.

Field of view		Pyramidal asymmetric
Line of sight	**Azimuth**	180 °
	Elevation	75 °
Aperture	**Azimuth**	±43 °
	Elevation	+15°/−10°
Geodetic coordinates	**Longitude**	−5.5911 °
	Latitude	37.16643 °
	Height	0.1423 km
Observation spacing		5 s

In order to generate more samples following an operational-like scenario, a new sample is created shifting the reference epoch by one day and repeating the previous list of steps again, applying different samples of the perturbations at each iteration. Once the complete population of estimated and predicted orbits is obtained, together with their covariance time-evolution, the covariance determination methodology previously explained can be applied to estimate the variance of the different consider parameters. The expected values of such variances correspond to those used in the simulation process, for the drag force, for the range bias, and for the space weather prediction, which are described in Section 3.4.

3.2. State vector components in the Mahalanobis distance

As previously discussed, one of the keys of the proposed methodology is the assumption that the Mahalanobis distance metric allows to include all orbital differences in the same theoretical χ^2 distribution. Under Gaussian and linear assumptions, the Mahalanobis distance for each orbit should remain approximately constant if the system errors are properly modeled.

Nonetheless, numerical instabilities were observed in the computation of the Mahalanobis distance when considering the complete state vector dimensions. These instabilities were tracked down to non-linearities that appeared in the position-velocity cross terms of the covariance matrix after

4 days of propagation, which caused ill-conditioning of the matrix and an exponential growth of the Mahalanobis distance in 1 principal component of the velocity. This same phenomenon was also seen in Sabol et al. (2010), where they attribute it to the inability of the Cartesian coordinates to maintain the Gaussianity. The connection between those non-linearities after propagation and OD characteristics such as observability, track length, orbit geometry or sensor network is a future line of research. Moreover, testing the proposed methodology in coordinates that maintain better the linearity such as equinoctial elements or curvilinear coordinates is a clear line of improvement.

However, other authors propose similar Mahalanobis distances and χ^2 distributions analysis where only position covariance is considered, arguing that position covariance realism is of higher relevance for high velocity collision risk assessments, which is one of the most common types of RSO encounters (Laurens et al., 2017). Additionally, the position-only Mahalanobis distance remains sufficiently stable for the circular orbits under analysis. Therefore, in the Mahalanobis distance computation of the work presented here, we consider components related to the position differences projected to TNW local frame. Carrying out the analysis in local frames aligned with the satellite motion provide further insight on the effect of the considered perturbations. The impact of this choice in the proposed methodology is assessed with the simulated scenario results shown in Section 4.

3.3. Reference state, dynamic and sensor model

This section will briefly state the simulated scenario settings used to conduct the work presented here. The initial reference state is described in Table 2, representing a LEO object at around 800 km altitude. The reference epoch is the starting epoch of the simulation scheme described above. The dynamic model characteristics are described in Table 3, and the simulated noise of the radar measurements during the track generation can be seen in Table 4.

3.4. Covariance determination configuration

3.4.1. Common tests characteristics

This subsection describes the common characteristics of the test cases conducted in this analysis. Special characteristics of the selected test cases for analysis are presented later in Table 6.

- **Analysis interval:** arc where the Mahalanobis distances are computed. In this case, from $t_0 + 4$ to $t_0 + 11$ days in a 1 day time-step, obtaining a total of 8 different analysis epochs for each orbit. Analysing multiple epochs in the propagation arc not only provides additional elements to the Mahalanobis distance population, but it also allows to provide a consider parameter variance representative of a wider arc. Though it may appear that different arbitrary points of the orbits are mixed in the same analysis, this is mitigated by the Mahalanobis distance concept, which normalizes the orbital differences with their covariance. The beginning of analysis interval is chosen at $t_0 + 4$ to let the atmosphere errors to dominate the covariance. Despite typical propagation arcs of LEO applications range up to $t_0 + 7$, it is relevant to include further propagation to properly characterize the proxies prediction error. Both the aerodynamic and the atmospheric proxies consider parameter models impact the aerodynamic drag force. Thus, a wider analysis window is crucial to discern the linear impact of the proxies consider parameter model (Eq. 16).
- **Time frame:** time step between each Monte Carlo sample. Set to 1 day forward shift, analogously to an operational scenario.
- **RMS rejection:** as customary in most statistical applications, a 3 RMS rejection criteria has been set on the Mahalanobis distance distribution, which on average has led to a 4% of rejection.

3.4.2. Simulated uncertainty

This subsection describes the simulated variances chosen for the different test cases, which are introduced into the simulations as explained in Section 3.1. All test cases in Section 4 contain the same perturbation levels for the aerodynamic and range bias consider parameter models, for benchmarking purposes, corresponding to:

- Aerodynamic model (σ_{AE}): 20%. This values is chosen as representative based on state-of-the-art studies, which state that around a 10–20% of uncertainty can be expected for the atmospheric density models (Vallado et al., 2014; International Reference Atmosphere COSPAR, 2012).
- Range bias (σ_{RB}): 20 m. This value has been chosen from operational scenarios expectations of previous analysis such as (Cano et al., 2021b).

Regarding the simulation of the uncertainty of the atmospheric proxies prediction, a preliminary analysis is conducted to assess the level of uncertainty expected in an operational scenario. We select an harmonic pulsation prediction model for the typical 11 years solar cycle. Starting at the beginning of the simulation scheme (2018–01-01), in time steps of 1 day, in a 1 year period, we obtain 11-days predictions of the solar proxies for each step. Then, we compare the prediction of $F_{10.7}$ and A_p proxies against the observed values (NOAA). The results are shown in Figs. 2 and 3 for the $F_{10.7}$ and A_p proxies, respectively. In the former one, despite an almost null mean, a linear growth of the 1σ value is appreciated, with a slope of 0.32%/day. This behaviour has led us to propose the linear growth model for the Proxies prediction model error of Section 2.3.3. In

Fig. 3, on the contrary, a constant 1σ absolute error of 8 units is observed for A_p.

However, the proposed linear model for the atmospheric proxies prediction error is applied in the aerodynamic force. To determine the impact that the observed proxies uncertainty supposes on the aerodynamic force, we introduce a perturbation equivalent to the observed 1σ values of $F_{10.7}$ and A_p for a single orbit propagation. These results are presented in Figs. 4 and 5. These figures represent the relative difference of drag acceleration between 2 orbits: an unperturbed orbit with the real proxies, and the second one including the 1σ level perturbations. In Fig. 4, only the $F_{10.7}$ proxy has been perturbed, observing also a linear acceleration difference evolution, of an order of magnitude similar to the slope of the $F_{10.7}$ proxy itself. However, when the A_p perturbation is also included as shown in Fig. 5, not only the slope is increased, but also a significant bias is obtained.

This analysis is useful to anticipate uncertainty levels expected in the presented simulation environment derived for the proxies prediction error, where the 1σ proxies uncertainty are translated in slopes of $1.35\%/day$ errors in the aerodynamic force. In light of these results, the following 2 cases have been considered to introduce the atmospheric proxies error in the simulations:

- Operational forecast: corresponding to the exact same forecast applied for the preliminary analysis, to be representative of operational prediction errors.
- Controlled proxies error: a simulated standard deviation of 3%/day is introduced with the proposed model of Section 2.3.3. The value is chosen to be of the order of magnitude of the expected variance of the real forecast as discussed above. This allows to test if the method is able to properly characterise the uncertainty in a scenario in which we have full control on the input perturbations, introducing them as in the proposed model similarly to the aerodynamic model and range bias perturbation.

4. Results

In this section, the results of selected tests cases are presented and analysed in relation to the effectiveness of the proposed covariance determination methodology to characterise the uncertainty of the system. The section is divided in 4 subsections. The first two discuss the results of the different test cases, the first one using the True reference orbit (Section 4.1) and and the second one applying the Operational reference orbit (Section 4.2). The third subsection presents a brief analysis on the accuracy of the

Table 6
Selected test cases characteristics and results.

Id	Consider Parameter Results	Accuracy $\lvert\%\rvert$	Metric	Relevant features
1	$\sigma_{AE} = 18.18\%$ $\sigma_{RB} = 21.8$ m $\sigma_{PE} = 3.64$ %/day	9.1 9 21	0.4	True reference CvM metric 500 samples Controlled PE
2	$\sigma_{AE} = 18.63\%$ $\sigma_{RB} = 20.01$ m $\sigma_{PE} = 3.19$ %/day	6.9 0.05 6.3	0.62	True reference CvM metric 1000 samples Controlled PE
3	$\sigma_{AE} = 18.24\%$ $\sigma_{RB} = 22.2$ m $\sigma_{PE} = 1.95$ %/day	8.8 11 -	0.86	True reference CvM metric 500 samples Op. forecast
4	$\sigma_{AE} = 19.69\%$ $\sigma_{RB} = 22.97$ m $\sigma_{PE} = 1.27$ %/day	1.6 14.9 -	1.5	True reference KS metric 500 samples Op. forecast
5	$\sigma_{AE} = 21.02\%$ $\sigma_{RB} = 24.73$ m $\sigma_{PE} = 0.00$ %/day	5.1 23.7 -	1.67	True reference CvM metric 500 samples Op. forecast without PE
6	$\sigma_{AE} = 19.49\%$ $\sigma_{RB} = 22.08$ m $\sigma_{PE} = 1.93$ %/day	2.6 10.4 -	0.82	Op. Ref. CvM metric 500 samples Op. forecast
7	$\sigma_{AE} = 19.52\%$ $\sigma_{RB} = 21.49$ m $\sigma_{PE} = 1.81$ %/day	2.4 7.5 -	1.68	Op. Ref. CvM metric 1000 samples Op. forecast

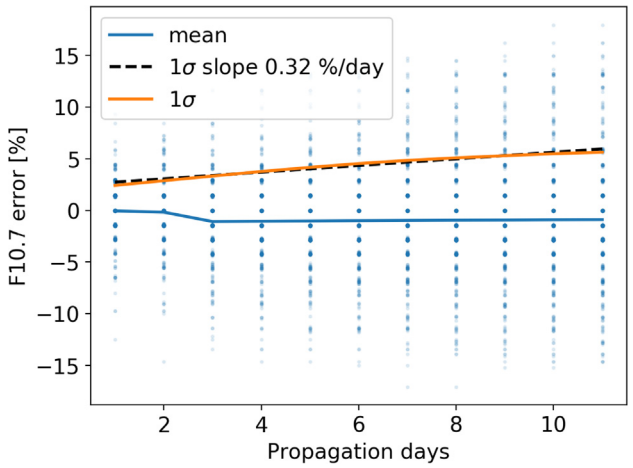

Fig. 2. F10.7 relative prediction error as a function of prediction time.

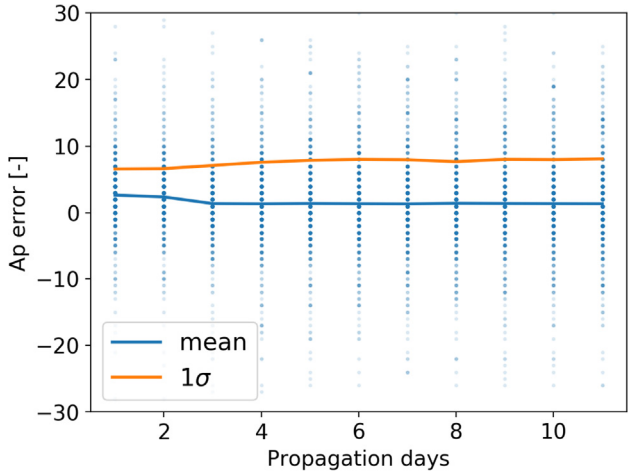

Fig. 3. Ap absolute prediction error as a function of prediction time.

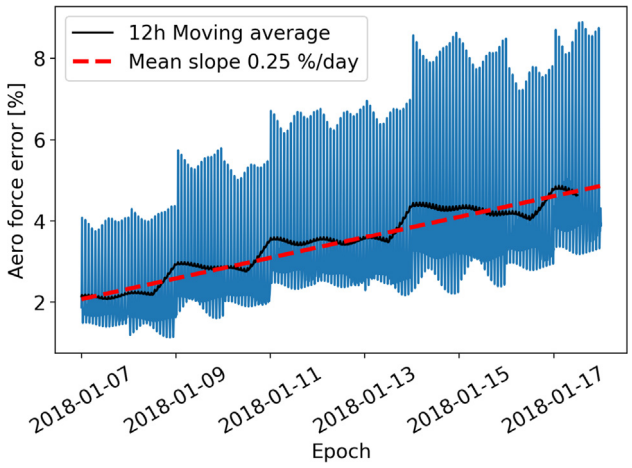

Fig. 4. Aerodynamic acceleration relative error with predicted $F_{10.7}$ 1σ perturbation.

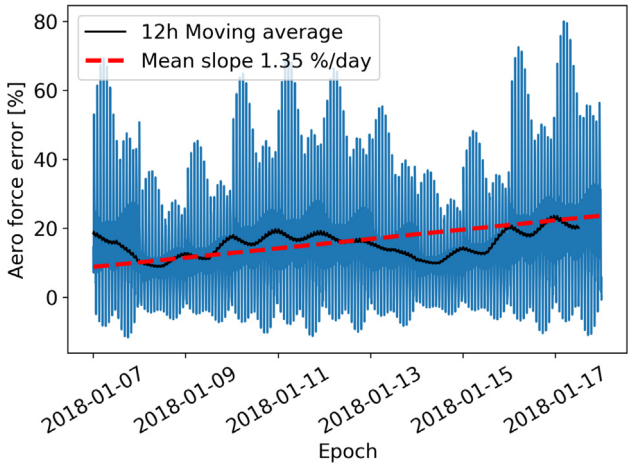

Fig. 5. Aerodynamic acceleration relative error with predicted $F_{10.7}$ 1σ and A_p 1σ perturbation.

methodology (Section 4.3). The last subsection discusses the performance of the covariance determination methodology in terms of covariance realism (Section 4.4).

Table 6 shows these results for 7 test cases, where the columns for each case correspond respectively to: 1) the identification number of each test case 2) the determined consider parameters standard deviation after applying the presented covariance determination process 3) the accuracy of the determined consider parameters standard deviation results as compared with the uncertainty introduced in the simulations 4) the final statistical comparison metric obtained 5) the relevant features of each case, such as the used reference, the chosen metric and the amount of Monte Carlos samples (i.e. orbits estimated and propagated). Let us explain the Relevant features column of Table 6. For each test, we are differentiating when the true reference orbit is used for the Mahalanobis distance computations or whether the previously defined Operational reference one is considered. Also, the chosen statistical metric is mentioned, either Cramer-von-Mises ("CvM") or Kolmogorov–Smirnov ("KS"). The amount of samples used during the computations is also shown. Finally, for each test case, the chosen option to introduce the atmospheric proxies prediction error is included, either the variance according to the proposed model ("Controlled PE") or the operational forecast ("Op. forecast"). Additionally, note that in the case of the proxies prediction consider parameter, accuracy is only provided for the controlled perturbations case, as only in such scenario we have a properly known target uncertainty.

4.1. True reference orbit

Test Case 1 uses the unperturbed true orbit as reference for the Mahalanobis distance computations, with 500 samples. As is seen in Section 4.3, this number has been selected as a compromise between having sufficient statistical samples for enough accuracy, but maintaining a realistic time-span (1.5 years approximately), which is relevant in

operational scenarios. In this test, the atmospheric proxies prediction error uncertainty has been introduced in the system with the fully controlled model. As observed in Table 6, an accuracy better than a 10% is obtained for the aerodynamic model error and range bias error, whereas a lower accuracy is found for the prediction error. As is further discussed later, the Cramer-von-Mises test statistic shows the lowest value of all test cases, pointing out a proper model matching between the actual uncertainty and the proposed models. Being able to characterize properly the different sources of uncertainty introduced in the system is an indicator of the ability of the covariance determination method to maintain the trace of the error sources, decoupling their impact on the orbits despite the methodology assumptions that neglected the correlation between the consider parameters and the analysed orbits.

Test Case 2 shares the same configuration as Test Case 1, with the controlled perturbation of the atmospheric proxies, but in this case increasing the samples up to 1000. This test case allows to demonstrate that the accuracy of the proposed methodology increases with the amount of samples, as would be expected, though further discussion about the accuracy of the method is provided in Section 4.3. Additionally, the Cramer-von-Mises metric still rejects the null hypothesis, maintaining a good fit between the system uncertainty and the proposed models as can be seen in Fig. 6. This figure shows the histogram of the final squared Mahalanobis distance distribution after applying the determined consider parameter variances, together with its empirical CDF as blue line. It also depicts the theoretical PDF and CDF of the χ^2 distribution of the corresponding DOF as red lines, as well as the empirical CDF of the distribution when no consider parameter correction is applied as a black line. This test case shows that the methodology is able to provide accurate results with a proper statistical matching when the system uncertainty is correctly modelled, as in this controlled case.

Test Case 3 shares again the same configuration as Test Case 1, but now applying the operational atmospheric forecast procedures. It can be noted that the consider parameter variances obtained with the proposed covariance determination methodology are representative of the introduced perturbation in the presented simulations. In both the aerodynamic model and range bias, the obtained results differ by less than a 11% to the target values (20% for σ_{AE}, 20 m for σ_{RB}). In terms of the Proxies prediction error, the method has determined a 1.95%/day, whose order of magnitude is similar to the expected uncertainty as discussed in Section 3.4.2 and observed in Fig. 5. Regarding the Cramer-von-Mises statistical comparison metric, a score of 0.86 is obtained, thus not rejecting the null hypothesis. The obtained squared Mahalanobis distance distribution is shown in Fig. 7. Overall, the distribution matches the expected χ^2 behaviour, despite being slightly overpopulated on the first quarter of the CDF, which is ultimately appreciated in the test metric, being larger than in Test Case 1. Recovering the χ^2 behavior is a direct indicator of covariance realism improvement, which is the main objective of the method. This indicates that the determined covariance is able to characterise the uncertainty of the system better than when no correction is applied. Although this is further analysed later via covariance containment tests, the CDF of the initial non-corrected squared Mahalanobis distance distribution is included in Fig. 7, for comparison. It can be clearly seen how the initial distribution is far from resembling a χ^2 behaviour, obtaining less than 5% of the population in the range showed in the figure. These remarkably large squared Mahalanobis distances in the

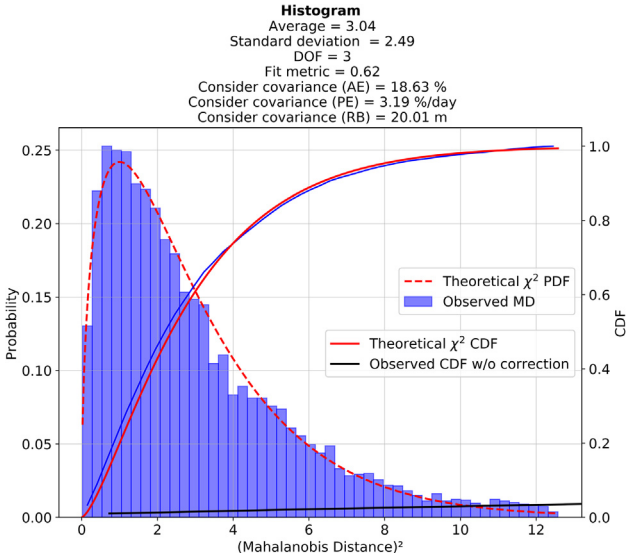

Fig. 6. Test 2. Squared Mahalanobis distance distribution with optimum consider covariance results.

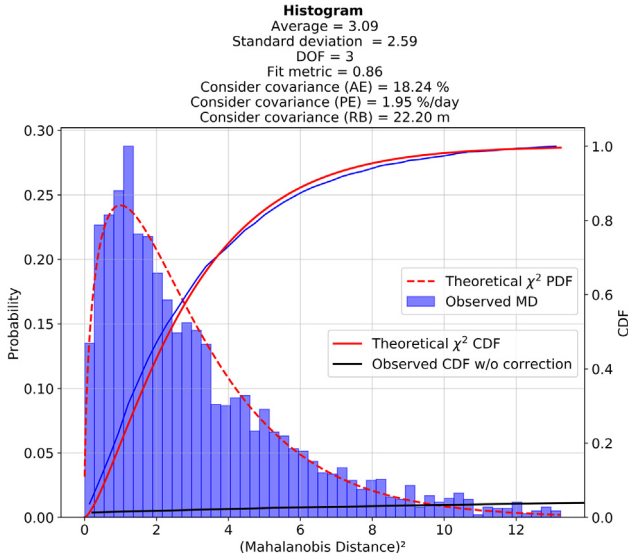

Fig. 7. Test 3. Squared Mahalanobis distance distribution with optimum consider covariance results.

non-corrected distribution are due to an overly optimistic size of the noise-only convariance.

Test Case 4 is analogous to Test Case 3 except for the optimisation metric used, in this case, Kolmogorov–Smirnov. The results of Table 6 point out that similar consider variances are obtained, indicating that both metrics arrive to similar results. A small trade-off between aerodynamic model uncertainty and proxies prediction uncertainty is observed in this case. Again, the obtained Kolmogorov–Smirnov metric does not allow to reject the null hypothesis.

Test Case 5 allows to show the benefits of upgrading the uncertainty model of the system. In this test case that shares the same characteristics as Test Case 3, no consider parameter correction for the Proxies Prediction error has been included. The obtained squared Mahalanobis distance distribution for this case can be seen in Fig. 8. The Cramer-von-Mises metric is above the threshold of 1.16, which rejects the null hypothesis that the population belongs to a χ^2 distribution. For further insight when only 2 consider parameters are present, a contour plot of the CvM metric as a function of both consider parameters is shown in Fig. 9. Here, the existence of a global minimum can be observed, corresponding to the optimum consider parameters found by the proposed methodology. However, the existence of such minimum does not ensure a correct statistical comparison, as is the case when the used models are not sufficient. This confirms that a better uncertainty characterisation is obtained when the solar prediction uncertainty is included as a consider parameter when predicted atmospheric weather forecasts are used. As expected, the better the uncertainty of the system is modelled, the better the proposed covariance determination method is able to improve the covariance realism. This highlights the relevance of properly modelling all sources of uncertainty in the space environment.

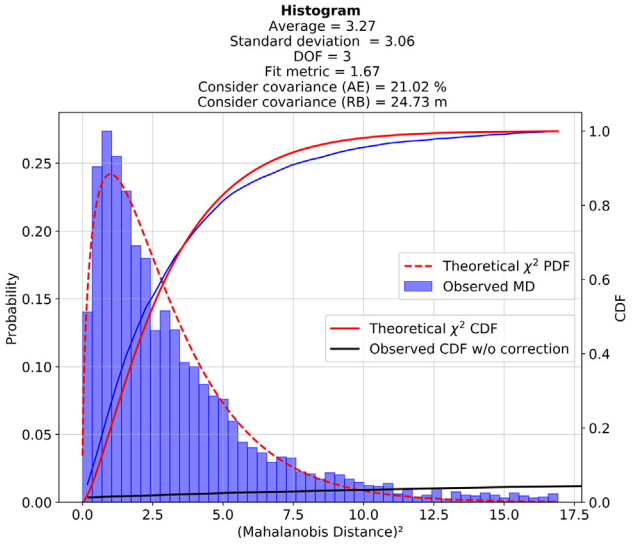

Fig. 8. Test 5. Squared Mahalanobis distance distribution with optimum consider covariance results.

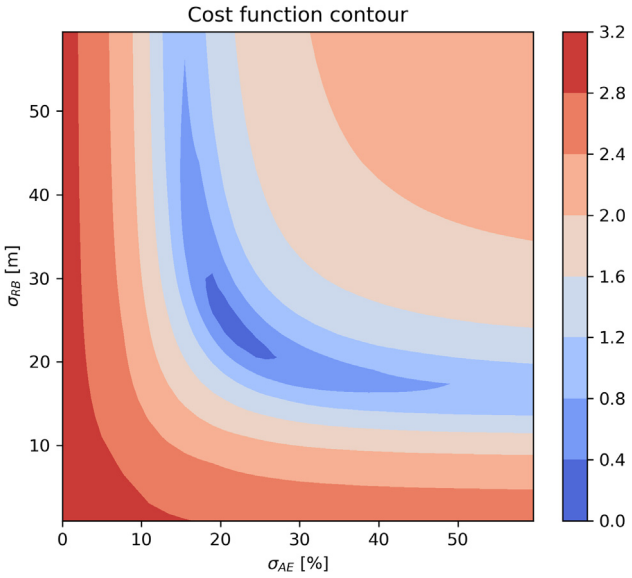

Fig. 9. Test 5. Cramer-von-Mises metric logarithmic contour as a function of aerodynamic model and range bias consider parameter standard deviations.

4.2. Operational reference orbit

Test Case 6 uses the Operational Reference orbit for orbital differences computations. The similarity of these results with the ones obtained in Test Case 3 indicates that the covariance determination is able to achieve satisfactory results without requiring an assumed perfect orbit. In an operational environment, this allows to use orbit determinations with observations during the propagation arc, not depending on external sources of precise ephemeris and showing the operational applicability of the proposed method in SSA operational environments. As was described previously, the uncertainty of such OD must be taken into consideration for a correct Mahalanobis distance computation. Even though in the chosen simulation scenario the operational references orbits did not contain any model error (only measurements error), the proposed methodology is able to cope with modelling errors in the operational reference orbit since, as explained in Eq. 18, the covariance of the reference orbit is also corrected by the consider parameter variances.

Finally, Test Case 7 has been included to show a benchmark with an increased number of orbits in the case of using both the Operational Reference orbit and the operational atmospheric proxies forecast. On the one hand, the accuracy of the optimum consider parameter variances is improved for the aerodynamic model and the range bias. Increasing the statistical population allows the method to better characterise the uncertainty, as was also seen in Test Case 2. On the other hand, the Cramer-von-Mises statistic obtained leads to the rejection of the null hypothesis. As can be seen in Fig. 10, the obtained distribution does not significantly deviates from the theoretical χ^2 behaviour. Nonetheless, the increased population allows the

Cramer-von-Mises test to have sufficient statistical evidence that the distribution does not match the χ^2 behaviour. This is attributed to a mismatch between the used model for the prediction of proxies and the one used in the covariance determination methodology. The fact that the statistical comparison in Test Case 2 is significantly better (see Fig. 6) points out that the proposed model for the atmospheric proxies prediction is not sufficient when the operational forecast procedure is applied. Recalling the analysis of Section 3, the introduced uncertainty had two differentiated sources, the $F_{10.7}$ Solar Flux and the A_p Geomagnetic Index. Though the retrieved consider covariance (σ_{PE}) is in line with the expectations derived from the $F_{10.7}$ uncertainty, the A_p uncertainty has not been characterized. Not tackling this non-negligible uncertainty source leads to the model mismatching showed on the metric.

4.3. Accuracy analysis

It has been seen in the previously discussed results that, as expected, the accuracy of the method improves when increasing the amount of samples included in the analysis. In this subsection, the accuracy of the covariance determination method is assessed in two different ways. Firstly, we assess the number of orbits (or samples) that are required by the statistical minimisation process. Fig. 11 shows the RMS of the accuracy achieved by the covariance determination method as a function of the number of orbits, in the simulation scenario of Test cases 1 and 2. Fig. 11 shows that the choice of the number of orbits to include in the analysis corresponds to a trade-off between accuracy and the amount of data available. When using approximately more than 700 orbits, an accuracy of the order of 5% is achieved. An accuracy of around 15% is expected in the range between 100–600 orbits, whereas it decreases significantly for less than 100 orbits, since not enough samples are available to characterise the uncertainty of the system.

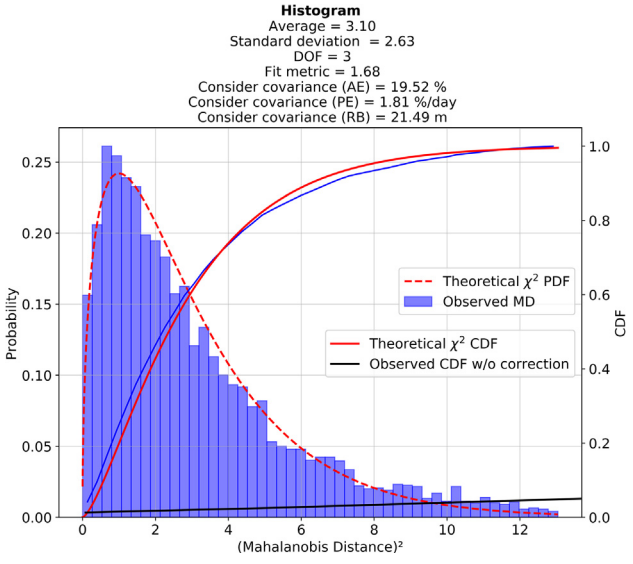

Fig. 10. Test 7. Squared Mahalanobis distance distribution with optimum consider covariance results.

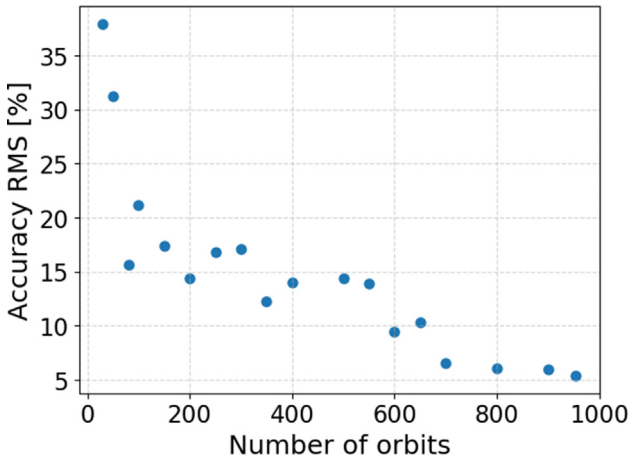

Fig. 11. Covariance determination method accuracy as a function of the number of orbits.

Secondly, the provided accuracy results presented in Table 6 correspond to a single execution of the simulation for each Test case scenario. However, this result would correspond to a "sample" of the method accuracy, since slightly different results may appear when repeating the simulations, applying different realizations of the perturbations and measurement noise. Table 7 shows the consider parameter variances results for test case 1 with 10 different seeds for the noise and perturbation generation.

Even though only 10 repetitions of the simulations have been carried out, these results provide insight on the expected standard deviation of the methodology accuracy. Extending this analysis to more repetitions and to the other test cases scenarios is proposed for future work. The mean values of the consider parameter variances are close to the target values, with the target value being included inside the standard deviation. The worst accuracy is found for the proxies prediction error, which is attributed to its coupling with the aerodynamic model error, which reduces its traceability. The mean of the accuracy RMS remains at

Table 7
Test cases 1 accuracy standard deviation.

N = 500	Computed σ			Accuracy RMS [%]
Seed	AE [%]	PE [%/day]	RB [m]	
1	18.18	3.64	21.80	14.36
2	18.76	3.35	21.37	8.59
3	21.35	2.97	20.95	4.80
4	20.77	3.83	19.42	16.21
5	19.53	3.60	19.41	11.75
6	21.83	3.06	19.98	5.41
7	20.19	3.24	20.23	4.70
8	19.01	3.52	21.21	10.98
9	19.99	3.57	19.17	11.23
10	18.92	3.62	19.37	12.47
Mean	19.85	3.44	20.29	10.05
std	1.22	0.28	0.85	4.16

10% even for 500 orbits, with a standard deviation of a 4%, which is considered satisfactory.

4.4. Covariance containment

Under Gaussian assumptions, if the observed squared Mahalanobis distance follows a χ^2 distribution, an improvement in the covariance realism would be directly achieved. In this respect, covariance containment tests such as the one proposed by (Wiesel, 2003) provide further physical insight and visual representation of the proposed methodology effectiveness. To evaluate if the covariance is representative of the orbital differences, the Mahalanobis distance can be used as a metric to see the amount of points that lay inside a $k\sigma$ ellipsoid ($k = 1, 2, 3, 4$) and compare it against the theoretical expected fraction for a multivariate Gaussian distribution of the same number of DOF. In the presented cases, it corresponds to 3 DOF (TNW position differences).

Test Case 6 results are chosen for this analysis due to a greater resemblance to an operational scenario, as it maintains a realistic amount of data, it uses the Operational reference for comparison and achieves sufficient accuracy. Figs. 12 and 13 depict the orbital differences in TNW for such test case for a 3σ ellipsoid using the noise-only covariance and the determined consider covariance, respectively. Those points laying outside the ellipsoid are marked as red dots, as green otherwise. Firstly, the covariance containment result in Fig. 13 is close to the expected theoretical containment of a 3 DOF Gaussian distribution (see Table 9), showing a remarkable enhancement of the covariance realism as opposed to the outstandingly low containment of the noise-only covariance of Fig. 12. Bear in mind that such test case contained orbital differences for a wide propagation interval.

This correction of the covariance realism, derived from the computed consider parameters variances, is clearly dominant in the Along-track uncertainty component, where the order of magnitude of orbital differences is several times greater than the other 2 components, the Normal

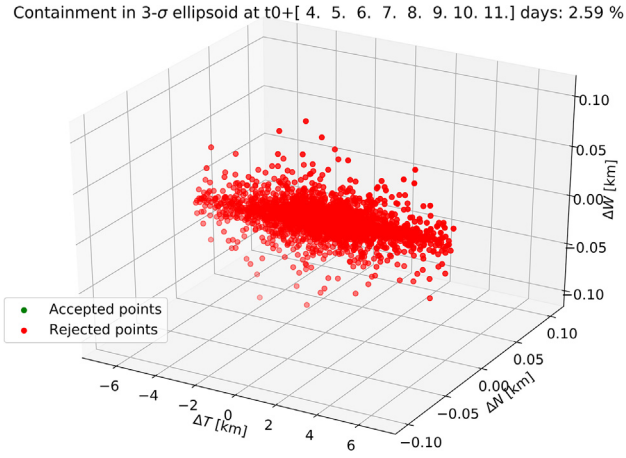

Fig. 12. Test 4. Noise-only covariance 3σ containment.

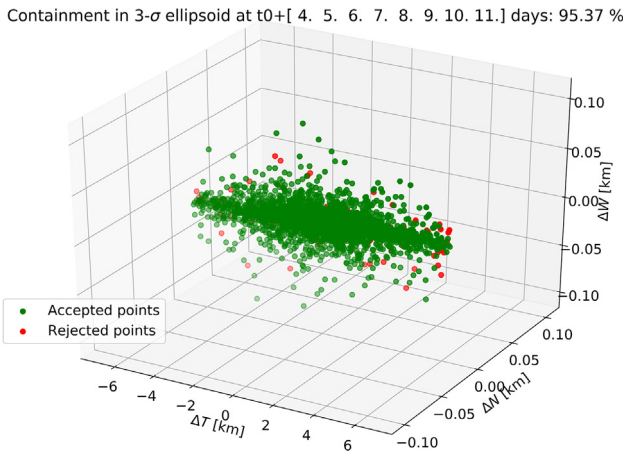

Fig. 13. Test 4. Consider covariance 3σ containment with determined consider parameter variances.

and Cross-track directions. This is the expected behaviour for LEO objects for the analysed error sources. The atmospheric drag force affects satellites on the direction of the velocity and thus both aerodynamic and proxies prediction errors are accumulated in the Along-track direction. Similarly, range-bias errors induce orbital differences in the direction of motion coinciding again with the Along-track direction in the nearly-circular orbit considered. We can distinguish three contributions to the covariance correction, recalling that the consider parameter correction is applied at estimation epoch:

- The aerodynamic model consider parameter variance affects mostly the drag coefficient covariance at estimation epoch, and such correction at estimation epoch is mapped into position covariance via the ESTM during the orbit propagation.
- The range bias variance affects the Along-track position and velocity covariance at estimation epoch, not affecting directly the propagation since it corresponds to a measurement model error. Of course, such initial inflation on position and velocity components will indeed impact the covariance propagation.
- The variance of the proxies prediction consider parameter does not provide any correction at estimation epoch, since there is no uncertainty on the proxies during the determination arc. However, the impact of this consider parameter is mapped to the position covariance due to the effect of the complete ESTM propagation.

Despite the observed increment of the covariance realism, it is relevant to analyse the improvement achieved at each analysed propagation epoch. The individual containment results for such epochs can be seen in Table 9 and its counterpart using the noise-only covariance in Table 8. All shown results share the common consider covariance correction using the optimum results of Test Case 6. A color scale has been added to facilitate the comparisons. Overall, as previously mentioned, the covariance realism provided

by the uncorrected noise-only covariance is significantly lower than the determined consider covariance, for the noise levels introduced in the presented simulations. It can be noted that the 3σ average containment of Table 9 differs slightly from the one showed in Fig. 13. The reason is the outliers rejection process. On the results showed in the figure, all data is analysed simultaneously, which causes the RMS rejection process to reject more data from conflicting epochs such as $t_0 + 11$ days, as is further explained below. These rejected outliers are not accounted for in the covariance containment, increasing slightly the containment percentage. On the contrary, the daily results of Table 9 have their own individual outlier rejection, leading to the slight differences observed between both results.

The individual containment results are, on average, around the expected theoretical results though presenting oscillations. This is expected since a singular consider parameters correction is aiming to correct the covariance at different propagation epochs simultaneously, whereas the uncertainty present in each of them is expected to vary. However, including all epochs in the same optimisation not only allows to provide the most representative solution for the interval, but also provides an additional amount of statistical population, facilitating the analysis. Two different regions of Table 9 are highlighted as reddish colours. First, the containment results at the 4^{th} propagation day are lower than expected for 1σ and 2σ ellipsoids. For short propagation periods, the estimation uncertainty is still relevant as compared to the covariance inflation introduced by the consider parameter correction, reducing the covariance realism enhancement of the methodology. Second, reduced covariance realism performance is observed at $t_0 + 11$ days. This is undoubtedly related to the inaccuracies of the solar proxies prediction model as was seen in Test Case 7. After long propagations, not only the linearity assumptions are stressed, but also the effect of the proxies prediction errors gain relevance as compared to the other sources. Therefore, not modelling such uncertainty perfectly is causing the containment at such regions to decay. However, it is important to highlight that long propagation arcs need to be included in the proposed covariance determination methodology so that the effect of the solar proxies prediction can be distinguished from the effect of the aerodynamic model error.

Table 8
Test 4. Noise-only covariance containment.

Epoch [days]	Without consider parameter correction [%]			
	1σ	2σ	3σ	4σ
t0+4	0	1.34	2.01	3.57
t0+5	0.45	1.12	2.01	3.58
t0+6	0	0.45	3.17	3.85
t0+7	0.68	1.81	2.71	4.52
t0+8	0	0.9	2.71	3.85
t0+9	0.44	1.98	2.86	4.4
t0+10	0.45	0.91	2.49	3.63
t0+11	0	1.35	2.7	4.5
Average	**0.25**	**1.23**	**2.58**	**3.99**
Theoretical (3DOF)	**19.9**	**73.9**	**97.1**	**99.87**

Table 9
Test 4. Consider covariance containment.

Epoch [days]	Applying consider parameter correction [%]			
	1σ	2σ	3σ	4σ
t0+4	16.2	67.8	94.03	100
t0+5	22.41	73.57	98.52	100
t0+6	20.13	73.38	96.32	100
t0+7	23.33	75.38	98.27	100
t0+8	19.96	69.75	96.14	100
t0+9	24.78	74.35	94.78	100
t0+10	20.22	69.11	93.11	99.56
t0+11	24.1	70.5	88.51	97.75
Average	**21.39**	**71.73**	**94.96**	**99.66**
Theoretical (3DOF)	**19.9**	**73.9**	**97.1**	**99.87**

5. Conclusions

This work has introduced a novel methodology to characterise the uncertainty in the space environment and improve the covariance realism. To this end, the consider parameter theory of batch least-squares methods has been applied in combination with Extended State Transition Matrix propagation to improve the covariance realism by means of the modelled consider parameters. This work focused on the aerodynamic model error, the range bias error and the error of the prediction of space weather proxies. The theoretical base to map the effect of the additional parameters in the covariance affecting both the estimation or the propagation arc has been developed. To compute the unknown variances of such parameters, a minimisation process has been proposed based on the comparison between the observed Mahalanobis distance distribution and its theoretical χ^2 behaviour under Gaussian assumptions, using predicted and estimated orbits to compute the orbital differences.

The results, obtained in a simulated scenario, showed that the proposed methodology is able to characterise the system uncertainty accurately for the aerodynamic model error, the range bias error and the atmospheric proxies prediction when the uncertainty present in the system follows the proposed models. A straightforward advantage of the proposed covariance determination method is that a physics-based traceability of the uncertainty sources is maintained. EDF statistics such as Cramer-von-Mises or Kolmogorov–Smirnov were successfully applied along the statistical comparison process, not only improving the method robustness as compared to previous studies

(Cano et al., 2021b; Cano et al., 2021a), but also providing direct information about the quality of the proposed uncertainty models. When applying the operational proxies forecast method, despite the clear improvement in the statistical comparison as opposed to not including it, the tests metrics showed that the observed squared Mahalanobis distance distribution diverged from the χ^2 distribution when sufficient statistical samples were included in the analysis. This is a clear line of improvement, mostly related to the characterisation of the A_p proxy uncertainty, highlighting the relevance of the uncertainty model for the proposed covariance determination methodology.

Furthermore, the method has provided accurate results when selecting the Operational reference orbit, this is, when using estimated orbits as reference to obtain the Mahalanobis distance instead of an unperturbed, "true" orbit. This is relevant for the operational scenarios aimed at, since generally, external data such as precise orbit products are not available for most satellites or space debris objects.

Finally, covariance containment tests have provided a clear visualisation of the covariance realism improvement achieved with the proposed covariance determination method as compared to the expected containment of a multivariate Gaussian distribution. The covariance is elongated mostly on the Along-track direction to accommodate the uncertainty present in the aerodynamic force. Overall, the obtained containment shows satisfactory accuracy to the theoretical containment results except on the beginning and end of the analysis arc. This is again a line of improvement, also related with the quality of the proposed uncertainty models.

Nonetheless, there is still a long road ahead. Apart from the proxies prediction model refinement to better characterise the effect of A_p proxy uncertainty, it is customary to move onto real data to completely assess the performance of the proposed method and consider parameters. Further analysis of the methodology accuracy standard deviation in different scenarios is also required for future research. Additionally, the Gaussian assumptions that represent the basis of this method should be revisited, widening the method for other distributions such as log-normal or Gauss-von-Mises, as well as more complex uncertainty models such as stochastic Brownian motion, Ornstein–Uhlenbeck, Gauss–Markov processes or even time–space correlations in atmospheric uncertainty.

Declaration of Competing Interest

The authors declare that they have no known competing financial interests or personal relationships that could have appeared to influence the work reported in this paper.

Acknowledgments

This project has received funding from the "Comunidad de Madrid" under "Ayudas destinadas a la realización de doctorados industriales" program (project IND2020/TIC-17539).

References

Alfriend, K., Wilkins, M., 2000. Covariance as an estimator of orbit prediction error growth in the presence of unknown sensor biases. Am. Astrono. Soc. 103, 99–422.

Cano, A., Fernandez, S., Pastor, A., Escobar, D., 2021a. Improving orbital uncertainty realism through covariancedetermination in GEO. In: 22nd Advances Maui Optical and Space Surveillance Technologies (AMOS) Conference.

Cano, A., Pastor, A., Escobar, D., 2021b. Covariance determination for improving uncertainty realism. In: 8th European Conference on Space Debris. ESA Space Debris Office.

Cerven, W., 2014. Improved empirical covariance estimation. Adv. Astronaut. Sci. 150, 879–895.

Cerven, W.T., 2011. Covariance error assessment, correction, and impact on probability of collision. In: AAS/AIAA Space Flight Mechanics Meeting.

D'Agostino, R.B., Stephens, M.A., 1986. Goodness-of-fit techniques. Vol. 68 of STATISTICS: Texbooks and Monographs. MARCEL DEKKER, INC, New York.

Duncan, M., Long, A., 2006. Realistic covariance prediction for the earth science constellation. In: AIAA/AAS Astrodynamics Specialist Conference and Exhibit. American Institute of Aeronautics and Astronautics.

Folcik, Z., Lue, A., Vatsky, J., 2011. Reconciling covariances with reliable orbital uncertainty. In: Advanced Maui Optical and Space Surveillance Technologies Conference, p. E34.

Frisbee, J.H., January 2011. An empirical state error covariance matrix for weighted least squares estimation method. Tech. Rep. JSC-CN-24133, NASA Johnson Space Center Houston, TX, United States. https://ntrs.nasa.gov/api/citations/20110014000/downloads/20110014000.pdf.

Hill, K., Sabol, C., Alfriend, K.T., 2012. Comparison of covariance based track association approaches using simulated radar data. J. Astronaut. Sci. 59 (1–2), 281–300.

International Reference Atmosphere COSPAR, 2012. Models of the earth's upper atmosphere. Tech. rep., Committee on Space research (COSPAR) International Reference Atmosphere.

Jazwinski, A., Jan. 1970. Stochastic processes and filtering theory. Vol. 64 of Mathematics in science and engineering. Academic Press, New York.

Junkins, J.L., Akella, M.R., Alfriend, K.T., 1996. Non-gaussian error propagation in orbital mechanics. J. Astronaut. Sci. 44, 541–563.

Laurens, S., Dolado, J., Cavallaro, G., Jouisse, M., Seimandi, P., Oct 2018. Towards the maintenance of Gaussianity on state vector uncertainty propagation. In: 69th International Astronautical Congress. Id: IAC-18, A6,9,3, x42351. https://iafastro.directory/iac/paper/id/42351/summary/.

Laurens, S., Seimandi, P., Couetdic, J., Dolado, J., 2017. Covariance matrix uncertainty analysis and correction. In: 68th International Astronautical Congress. Id: IAC-17,A6,7,2,x37415. URL https://iafastro.directory/iac/paper/id/37415/summary/.

Lopez-Jimenez, S., Pastor, A., Escobar, D., 2021. Improving orbital uncertainty realism through covariance determination. Acta Astronaut. 181, 679–693, URL https://www.sciencedirect.com/science/article/pii/S0094576520305658.

Mahalanobis, P., 1936. On the generalised distance in statistics. Proc. National Inst. Sci. India 2, 49–55.

McCabe, J.S., DeMars., K.J., 2014. Particle filter methods for space object tracking. In: AIAA/AAS Astrodynamics Specialist Conference. American Institute of Aeronautics and Astronautics (AIAA), San Diego, CA.

Michael, J.R., 1983. The stabilized probability plot. Biometrika 70 (1), 11–17.

Montenbruck, O., Gill, E., 2000. Satellite Orbits: Models, Methods and Applications. Springer-Verlag, Berlin Heidelberg, Berlin.

Poore, A.B., Aristoff, J.M., Horwood, J.T., Armellin, R., Cerven, W.T., Cheng, Y., Cox, C.M., Erwin, R.S., Frisbee, J.H., Hejduk, M.D., Jones, B.A., Di Lizia, P., Scheeres, D.J., Vallado, D.A., Weisman, R. M., Jun. 2016. Covariance and Uncertainty Realism in Space Surveillance and Tracking. Tech. rep., Numerica Corporation Fort Collins United States. URL https://apps.dtic.mil/docs/citations/AD1020892.

Royston, P., 1993. Graphical detection of non-normality by using michael's statistic. Appl. Stat. 42 (1), 153.

Sabol, C., Sukut, T., Hill, K., Alfriend, K., Wright, B., Li, Y., Schumacher, P., 2010. Linearized orbit covariance generation and propagation analysis via simple monte carlo simulations (preprint). Adv. Astronaut. Sci. 136, 22.

Schiemenz, F., Utzmann, J., Kayal, H., 2019. Least squares orbit estimation including atmospheric density uncertainty consideration. Adv. Space Res. 63 (12), 3916–3935.

Schubert, M., Kebschull, C., Horstmann, S., 2021. Analysis of different process noise models in typical orbitdetermination scenarios. 8th European Conference on Space Debris, vol. 8. ESA Space Debris Office, Darmstadt, German.

Storn, R., Price, K., 1997. Differential evolution - a simple and efficient heuristic for global optimization over continuous spaces. J. Global Optim. 11, 341–359.

Tapley, B.D., Schutz, B.E., Born, G.H., 2004. Statistical Orbit Determination. Elsevier Academic Press, San Diego, California.

Vallado, D.A., 1997. Fundamentals of Astrodynamics and Applications, forth Edition. Space Technology Library. Springer and Microcosm Press, Hawthorne, CA.

Vallado, D.A., Alfano, S., 2011. Curvilinear coordinates for covariance and relative motion operations. In: AAS/AIAA Astrodynamics Specialist Conference. AAS, pp. 11–464.

Vallado, D.A., Finkleman, D., 2014. A critical assessment of satellite drag and atmospheric density modeling. Acta Astronaut. 95, 141–165.

Vallado, D.A., Kelso, T., 2013. Earth orientation parameter and space weather data for flight operations. In: Advances in the Astronautical Sciences. vol. 148. AAS 13–373.

Vasile, M., 2019. Practical Uncertainty Quantification in Orbital Mechanics. Springer International Publishing, Cham, pp. 291–328. https://doi.org/10.1007/978-3-030-20633-8_7.

Wiesel, W., 2003. Modern Orbit Determination. Aphelion Press, Beavercreek, OH.

Zanetti, R., D'Souza, C., 2013. Recursive implementations of the schmidt-kalman 'consider' filter. J. Astronaut. Sci. 60, 672–685.